

# Scaling dependence on the fluid viscosity ratio in the selective withdrawal transition

Itai Cohen

January 2002

## Abstract

In the selective withdrawal experiment fluid is withdrawn through a tube with its tip suspended a distance  $S$  above a two-fluid interface. At sufficiently low withdrawal rates,  $Q$ , the interface forms a steady state hump and only the upper fluid is withdrawn. When  $Q$  is increased (or  $S$  decreased), the interface undergoes a transition so that the lower fluid is entrained with the upper one, forming a thin steady-state spout. Near this transition the hump curvature becomes very large and displays power-law scaling behavior. This scaling allows for steady-state hump profiles at different flow rates and tube heights to be scaled onto a single similarity profile. I show that the scaling behavior is independent of the viscosity ratio.

## 1 Introduction

A look at Edgerton's photographic sequences of dripping faucets (see, for example, Edgerton *et al.* (1937)) should instantly convince any skeptic that there is something fascinating about a fluid interface changing its topology which hints at the richness of the underlying physics. Much attention has been devoted towards trying to classify these topological transitions in fluid systems (see, Caffisch & Papanicolaou (1993); Bertozzi *et al.* (1994); Goldstein *et al.* (1993); Pugh & Shelley (1998)) in the same manner as one classifies thermodynamic transitions. It has been shown that when the topological transition involves the formation of a singularity in the fluid flows or interface shapes, as is the case with a drop dripping from a faucet, one can use the singularity to organize studies of the transition systematically (see, for example, Barenblatt (1996); Lister & Stone (1998); Cohen & Nagel (2001)). As the singularity is approached, the separation between the length scales characterizing the boundary conditions and the length scales characterizing the system grows. Furthermore, the fluid systems can enter an asymptotic regime where a subset of the terms in the governing equations dominate the flows. The organization of the transition studies involves the identification of the different subsets of terms which can balance as the singularity is approached. In these asymptotic regimes, the systems

typically display scaling of length scales or other physical quantities and often, the interfacial profiles near the singularity can all be collapsed onto a universal curve. In many systems these singularities manifest themselves in the transition dynamics (see, Lister & Stone (1998); Bensimon *et al.* (1986); Nagel & Oddershede (2000); Zeff *et al.* (2000).) Here, this approach is extended to the study of the steady-state interface profiles near the topological transition associated with the industrially important (see, for example, Muskat (1972); Bear (1972); Cohen *et al.* (2001); Ganan-Calvo (1998)) process of selective withdrawal.

In the selective withdrawal experiment a tube is immersed in a filled container so that its tip is suspended a height  $S$  above an interface separating two immiscible fluids (figure 1). When fluid is pumped out through the tube at low flow rates,  $Q$ , only the upper fluid is withdrawn. The flows deform the interface into an axi-symmetric steady-state hump with a stagnation point at the hump tip (Fig. 1). The hump grows in height and curvature as  $Q$  increases (or  $S$  decreases) until the flows undergo a transition where the lower fluid becomes entrained in a thin axi-symmetric spout along with the upper fluid. The interface becomes unbounded in the vertical direction, the stagnation point moves from the hump tip into the interior of the lower fluid, and the upper fluid geometry becomes toroidal thus changing the topology of the steady state. Once the spout has formed, an increase in  $Q$  (or decrease in  $S$ ) causes the spout to thicken.

Near the transition, the steady-state mean radius of curvature at the hump tip,  $1/\kappa$ , can be orders of magnitude smaller than the length scales characterizing the boundary conditions (for example the tube diameter,  $D$ ). However, for the range of parameters explored thus far, even when the system is arbitrarily close to the transition,  $\kappa$ , while large, remains finite. The manifestation of a true singularity would entail the divergence or vanishing of some physical quantities or length scales describing the system. In practice, for all physical systems the approach to the singularity is cut off at some length scale. For the selective withdrawal system where both fluids have a viscosity of about 2 St, Cohen & Nagel (?) show that the cutoff appears when the mean radius of curvature at the hump tip is about  $200 \mu\text{m}$  which is well above the breakdown limit for the Navier-Stokes equations. It is still unclear which physical parameters determine this relatively large length scale for the hump mean radius of curvature cutoff,  $1/\kappa_u$ .

Nevertheless, fixing  $S$  and looking at the steady-state profiles as  $Q$  is increased, Cohen and Nagel observe that, up until the cutoff, both the hump curvature and height display scaling behavior characteristic of systems approaching a singularity. Furthermore, they are able to use the observed scaling relations to collapse the hump profiles near the transition onto a universal curve. In doing so, they have shown that it is possible to treat this as a “weakly-first-order” transition and use the same systematic approach others have successfully applied to the study of the drop snap-off problem<sup>1</sup>. However, understanding how to con-

---

<sup>1</sup>While scaling has been hypothesized by Acrivos & Lo (1978) for an analogous 3-D system it was never shown experimentally.

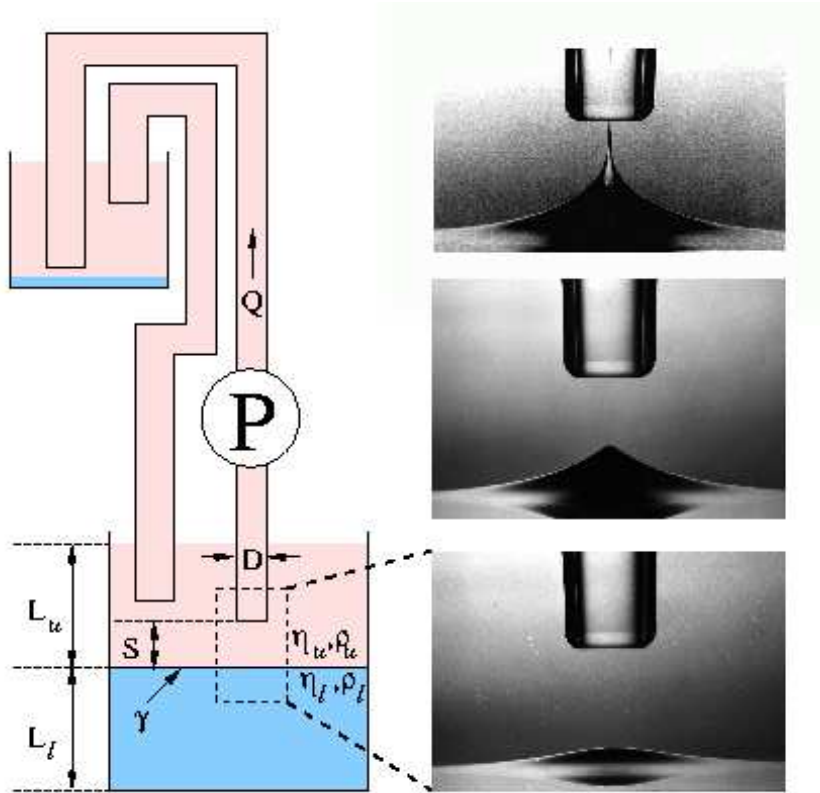


Figure 1: Diagram of the experimental apparatus and photographs of the steady state interface at different  $Q$ . Fluid is withdrawn from the withdrawal container and deposited into a waste container. The upper fluid is then siphoned back into the withdrawal container. As shown in the diagram, the parameters for this problem include the height of the tube from the interface,  $S$ , withdrawal rate,  $Q$ , surface tension,  $\gamma$ , fluid densities,  $\rho_u$  and  $\rho_l$ , fluid viscosities,  $\eta_u$  and  $\eta_l$ , tube diameter,  $D$ , fluid height above the interface,  $L_u$ , fluid height below the interface,  $L_l$ , container size, and surfactant concentration. Viewed bottom to top, the photographs show the evolution of the steady state interface as  $Q$  is increased. The top photograph of the interface in the spout state is taken from Cohen *et al.* (2001). The middle photograph of the hump at the transition flow rate is taken from Cohen & Nagel (?).

trol the cutoff curvature is crucial for obtaining a more accurate scaling analysis. Moreover, a precise understanding of the transition would allow for control of the minimum spout diameter. This control could, in turn be used to advance new emerging technologies such as coating micro-particles (Cohen *et al.* (2001)), creating mono-dispersed micro-spheres (Ganan-Calvo (1998)), and emulsification through tip streaming (Eggers (1997); Sherwood (1984)) which take advantage of the selective withdrawal geometry.

Further insight into this cutoff behavior is gained by comparing with an analogous two-dimensional (2-D) problem which roughly corresponds to replacing the tube with a line sink. Jeong & Moffatt (1992) showed that in an idealized case where the bottom fluid is inviscid while the top fluid is very viscous, the 2-D hump interface forms a two-dimensional cusp singularity beyond sufficiently high withdrawal rates. Recently, Eggers (2001) showed that when the lower fluid has a finite viscosity, the solution to the governing equations changes and the system no longer manifests a singularity. Instead, the approach to the singularity is cut off and the system undergoes a transition to a different steady state. In this new state, a sheet of the lower fluid is entrained along with the upper fluid into the line sink. However, the finite lower fluid viscosity prevents the hump profiles from scaling onto a similarity solution. In contrast, Cohen & Nagel (?) point out that even though they performed their experiments for 3-D selective withdrawal with an upper and lower fluid which were comparably viscous (about 2 St), they still observe scaling behavior and profile collapse onto a similarity solution. Whether or not performing the experiments with a lower fluid which is less viscous will allow the system to get closer to the singularity (as is the case in the 2-D analogue) has so far remained a mystery. In the present paper, a systematic analysis of the role which the lower fluid viscosity,  $\eta_l$ , plays in the selective withdrawal transition shows that neither  $\eta_l$  nor the viscosity ratio affect the scaling dependence of the hump profiles and the value of the cut-off curvature  $\kappa_u$ .

In addition to studying the various scaling dependencies, Cohen & Nagel (?) map out the location of the transition in the  $S$  vs.  $Q$  parameter space. Indeed, this topic is by far the most common feature of the selective withdrawal transition discussed in the literature. Yet, even this seemingly benign subject has its subtleties. For example, the experiments of Blake & Ivey (1986), Jirka & S. (1979), Harellman *et al.* (1959), and others used two fluids which had different densities but were miscible. However, as pointed out by Lister (1989), when surface tension is absent, there is always some fraction of the lower fluid which is extracted so that those experiments were not tracking the actual withdrawal transition<sup>2</sup>. Cohen and Nagel's studies of a pair of immiscible fluids which are comparable in their viscosity (about 2 St) are the first to take into account the effects of the surface tension in experiments mapping out the transition location for low Reynolds number flow. In this paper, these studies are extended to other fluid combinations. Once again, I find that neither  $\eta_l$  nor the viscosity ratio

---

<sup>2</sup>While these experiments did not track the transition, they may have been sufficient for their intended purpose of modeling magma layer mixing during volcanic eruptions.

affect the values of  $S$  and  $Q$  at which the transition occurs.

The paper is organized as follows: Section 2 describes the fluids and experimental apparatus used to make the measurements. This section also describes the effects of the container walls and fluid layer thickness on the transition. Section 3 addresses the hysteretic nature of the transition. Also addresses is the correlation between the amount of hysteresis and the final value for the hump curvature,  $\kappa_u$ , when the transition takes place at low enough values of  $S$ . In section 4 a scaling analysis is performed for a system which is identical to that used by Cohen and Nagel with the exception that the viscous lower fluid is replaced with one which is two hundred times less viscous. The two sets of results are then compared. In section 5, I map out the location of the selective withdrawal transition in the  $S$  vs.  $Q$  parameter space as a function of the upper and lower fluid viscosities. Also presented is a comparison of the experimental results with the theoretical prediction of Lister (1989) for the transition dependence on the parameters  $S$  and  $Q$ . Section 6 presents a discussion of the results. Finally, the role of surfactants is addressed in Appendix A. Since it is extremely difficult to keep a fluid interface free of surfactants it is important to isolate and control their effects. In the current studies the effects on the experimental results are found to be rather benign.

## 2 Characterization of Fluids and Experimental Details

As shown in figure 1, the parameters important for this experiment are the upper and lower fluid viscosities and densities ( $\nu_u, \nu_l, \rho_u, \rho_l$ ), the interfacial tension ( $\gamma$ ), the orifice diameter ( $D$ ), the height of the orifice ( $S$ ), the flow rate ( $Q$ ), the fluid height above the interface ( $L_u$ ), the fluid layer thickness below the interface ( $L_l$ ), the container size, and the surfactant concentration. In order to look at the scaling of the steady-state profiles, care must be taken in designing an experimental apparatus capable of isolating the profiles near the transition. Figure 1 displays a diagram of the apparatus in which the experiments were performed. A large tank (30 cm  $\times$  30 cm  $\times$  30 cm) capable of holding fluid layers that were each about 12 cm in height is used as the withdrawal container for the fluids. During the experiments, fluid is pumped out of the withdrawal container and into a waste container. When the system is in the spout state the fluids enter the waste container as an emulsion. This emulsion is deposited at the bottom of the waste container which is where the droplets comprised of the lower fluid remain. The upper fluid is siphoned back into the withdrawal container through large tubes at a rate which matches the withdrawal rate thereby keeping constant the upper fluid layer thickness in the withdrawal container. Note that the bottom fluid layer does not change its thickness when the system is in the hump state and decreases its thickness with time when the system is in the spout state. However, even for thick spouts (0.1 mm) and for large flow rates (10 ml/sec) the lower fluid layer decreases its thickness at the very slow rate of

0.01 mm/min which corresponds to a 0.1% change in the straw height,  $S$ .

The fluids were withdrawn using a B9000 Zenith metering gear pump attached to a variable speed DC motor. A Dynapar Rotopulser encoder was used to read out the withdrawal rate. The pump uses gears to displace fluid from the pump intake to the pump outlet. There are small variations in flow rate associated with the filling and draining of the gaps between the gear teeth. However, at large flow rates, or equivalently at high rotation frequencies, these variations damp out and the amplitude of the remaining noise corresponds to a very small percentage of the total flow rate. High rotation rates also average out the fluctuations in the driving motor. Using bigger or smaller pump attachments allows for pumping of the fluid at the same flow rate but at a different gear rotation rate. This allows for the determination of the effects of noise in the flow rate on the transition. A further reduction of the noise in the experiments is achieved by siphoning the fluids into the waste container. However, when siphoning, the maximum rate of withdrawal (determined by the viscosity, straw diameter, transfer tube length, transfer tube diameter, and fluid height difference between the withdrawal and waste containers) is substantially smaller.

The fluids used were heavy mineral oil (HMO), light mineral oil (LMO), silicone oil (polydimethylsiloxane or PDMS), salt water (Salt H<sub>2</sub>O), and mixtures of glycerin and water (Water/Glycerin). No surface chemistry was observed at the two-fluid interfaces even when the liquids remained in contact for periods longer than a month. However, a slight change in the transition flow rate at fixed  $S$  over a period of days indicated that the surfactant concentration at the interface was increasing with time. A detailed discussion of the surfactant effects appears in Appendix A. The viscosity,  $\nu$ , was measured using calibrated Cannon Ubbelohde viscometers immersed in a Cannon constant temperature bath. In this manner the viscosity could be determined to within  $\pm 5\%$ . Glycerin can be diluted with water so that the resultant fluid has  $0.01 \leq \nu \leq 9.8$  St (Segur & Oberstar (1951)). Table 1 lists the values of the viscosities and densities for the different fluids.

The surface tension,  $\gamma$ , of the two-fluid interface was determined using the pendant drop method (see, for example, Neumann & Spelt (1995); Hansen & Rodsrud (1991)) which takes advantage of the competition between the surface tension and buoyant forces acting on a static drop hanging from a nozzle. The buoyant forces distort the drop from a spherical shape. Measuring the distortion and density mismatch allows a determination of the surface tension. Implementation of this technique on water, toluene, and di-methylformamide showed a capability for measuring the surface tensions to within  $\pm 10\%$ . Table 1 lists the values of  $\gamma$  for the different fluids.

The apparatus was illuminated from the rear and a CCD video camera was used to image silhouettes of the steady state hump shapes. The images were transferred onto a PC where an edge tracing IDL program tracked and recorded the points where the derivative of the pixel intensity profile across the hump interface was extremized. The profiles were then superimposed onto the original images and checked for accuracy. In order to determine the mean curvature at the hump tip,  $\kappa$ , a Gaussian function was used to fit the tip of the recorded

	System 1	System 2	System 3	System 4	System 5	System 6	System 7
Upper Fluid	PDMS	PDMS	PDMS	PDMS	HMO	HMO	LMO
Lower Fluid	H <sub>2</sub> O	Salt H <sub>2</sub> O	Water/Glycerin	Glycerin	H <sub>2</sub> O	Water/Glycerin	H <sub>2</sub> O
$S_u$ Symbol	●	+	□	◆	○	▼	▲
$\gamma$ (dynes/cm)	43	40	29	23	35	31	34
$\rho_u$ (g/ml)	0.97	0.97	0.97	0.97	0.87	0.87	0.85
$\rho_l$ (g/ml)	1.00	1.11	1.24	1.26	1.00	1.24	1.00
$\Delta\rho$ (g/ml)	0.03	0.14	0.27	0.29	0.13	0.37	0.15
$\nu_u$ (cm <sup>2</sup> /s)	10	10	10	10	1.9	1.9	0.57
$\nu_l$ (cm <sup>2</sup> /s)	0.010	0.012	2.3	9.8	0.010	2.3	0.010
$\nu_l/\nu_u$	$9.5 \times 10^{-4}$	$1.1 \times 10^{-3}$	$2.1 \times 10^{-1}$	$9.3 \times 10^{-1}$	$5.3 \times 10^{-3}$	1.2	$1.8 \times 10^{-2}$
$\kappa_{usat}$ (1/cm)	$12 \pm 3$	$27 \pm 7$	$22 \pm 5$	$25 \pm 5$	$31 \pm 7$	$48 \pm 10$	$5 \pm 1$
$\alpha$	0.44	0.42	0.41	0.40	0.32	0.30	0.30

Table 1: List of the properties for each fluid system studied. Row 1 and 2 list the fluids used. Row 3 lists the symbols used in plotting the experimentally measured  $S_u$  curves in figures 12, 13, 4, and 6. Rows 4 through 10 list the values of the fluid parameters measured for the different systems. The second to last row shows the asymptotic value at which the mean curvature saturates,  $\kappa_{usat}$ , and the last row lists the power-law exponent  $\alpha$  used in fitting the experimentally measured  $S_u$  curves in figures 12, 13, 4, and 6

hump profile. The value of  $\kappa$  is taken to be the curvature of the fitting function at the hump tip.

Using this apparatus, I tested the effects of the container walls and thickness of the upper fluid layer on the transition flow rate,  $Q_u$ . Figure 2 shows a plot of the transition flow rate  $Q_u$  vs. the distance  $L_w$  from one of the container walls while the straw height,  $S$ , is held constant. The fluid parameters for this particular experiment correspond to those of system 3 in Table 1. When the straw is farther than about 2 cm from the container wall, there is no variation in the transition flow rate. Figure 3 shows a plot of the transition flow rate  $Q_u$  as a function of the upper fluid layer thickness  $L_u$  for constant  $S$ . The fluid parameters for this particular experiment correspond to those of system 5 in Table 1. As  $L_u$  is increased,  $Q_u$  first increases but eventually saturates and remains constant for  $L_u$  greater than about 3cm. In all of the experiments, the bottom fluid layer thickness  $L_l$  was typically kept at about 12 cm. Measurements of the transition flow rates showed no significant variations between systems with an  $L_l$  of 12, 10, and 6 cm. Similar measurements for the  $Q_u$  dependence on  $L_w$ ,  $L_u$ , and  $L_l$  were conducted for all of the different fluid combinations used in the experiments. For the tube diameters ( $D = 0.16$  cm and  $D = 0.79$  cm), tube heights ( $0.07$  cm  $< S < 2.0$  cm), and flow rates ( $Q < 20$  ml/sec) used in the experiments, the container walls were always sufficiently distant and the fluid layers were always sufficiently thick so as not to affect the flows.

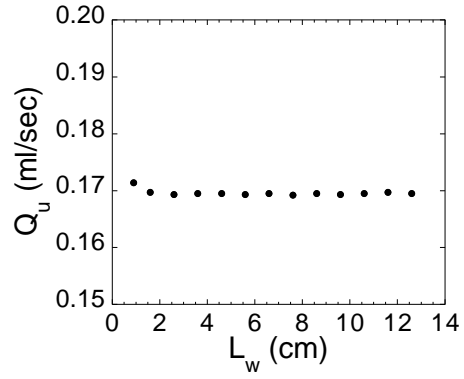


Figure 2: Plot of the transition flow rate,  $Q_u$  as a function of the distance between the withdrawal tube and the container wall,  $L_w$  for system 3 in Table 1. Beyond 2 cm,  $Q_u$  shows no dependence on  $L_w$ . Note that the Value of  $Q_u$  is plotted on a linear scale.

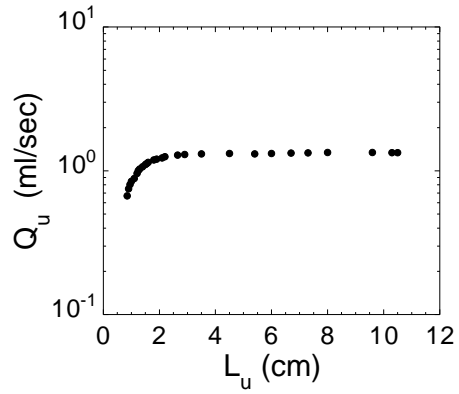


Figure 3: Plot of the transition flow rate,  $Q_u$  as a function of the upper fluid layer thickness,  $L_u$  for system 5 in Table 1. Beyond 3 cm,  $Q_u$  shows no dependence on  $L_u$ .



### 3 Transition Structure and Hysteresis

In their paper, Cohen & Nagel (?) map out the location and structure of the selective withdrawal transition for a pair of fluids corresponding to system 6 in table 1. Here I review these results and note that all of the fluid systems in table 1 display the same qualitative features. Much of our understanding of the selective withdrawal transition can be conveyed by focusing on the effects of the parameters  $S$  and  $Q$ . By fixing  $Q$  and tracking the hump profiles the tube height below which the interface forms a spout,  $S_u$ , can be determined. Figure 4 (taken from Cohen & Nagel (?)) shows that  $S_u \propto Q^{0.30 \pm 0.05}$  (A detailed discussion of how this result changes with the various fluid parameters along with a comparison to currently available theory is presented in section 5). As mentioned in the introduction, for the entire range of parameters explored thus far, the evolution of the steady state hump profiles is cut off by the hump to spout transition before  $\kappa$  diverges. However it is possible that there is more than one mechanism that is responsible for the transition cutoff. If this is the case it is important to isolate the regimes over which particular mechanisms dominate. The cut-off suggests that the transition may be hysteretic. Indeed, for transitions occurring at low  $Q$ , or equivalently at small  $S_u$ , the straw height at which the spout decays back into a hump is different from  $S_u$ . The difference of the two heights or hysteresis is defined as  $\Delta S$ . Figure 4 shows that  $\Delta S$  decreases exponentially with the flow rate  $Q$ . For this particular system the hysteresis can be fit with the function:  $\Delta S = 0.04 \exp^{-Q/0.032}$ . For  $Q > 0.1$  ml/sec,  $\Delta S$  was too small to measure. Figure 4 also shows how the hump mean radius of curvature,  $1/\kappa_u$ , and height,  $h_u$ , at the transition vary with  $Q$ . The dramatic decrease in  $\Delta S$  coincides with the onset of a flat asymptotic dependence for  $1/\kappa_u$  at  $Q > 0.1$  ml/sec. In order to quantify this correlation, the curvature data is fit with the form  $1/\kappa_u = 0.02 + 0.32 \exp^{-Q/0.032}$  which has the same exponential decay with  $Q$  as does the hysteresis. The curvature saturation values,  $\kappa_{usat}$ , for all of the systems are shown in the second to last row in Table 1.

A diagram (Hale & Cocak (1991)) summarizing the features of the transition is shown in figure 5. The vertical axis labeled  $q$  relates how much of the lower fluid is withdrawn as a function of the total fluid withdrawal rate  $Q$  and straw height  $S$ . The states accessible to the system are represented by a sheet which is embedded in this three dimensional parameter space. The part of the sheet which corresponds to the system in the hump state is located in the  $q = 0$  plane. An experiment where the flow rate is held fixed and the straw height is slowly reduced would correspond to a path which traverses the sheet in a direction which is parallel to the  $S$  axis. The fold in the sheet represents the hysteresis in the transition. As the straw height is reduced, the system runs out of hump states and makes a discontinuous jump at  $S = S_u$  (depicted by the dashed arrow pointing upward) to a part of the sheet which has a finite value of  $q$ . If  $S$  is reduced further, the sheet slopes towards higher values of  $q$  and more of the lower fluid is withdrawn. If on the other hand,  $S$  is increased, the system remains on the upper branch of the sheet until the spout states run out

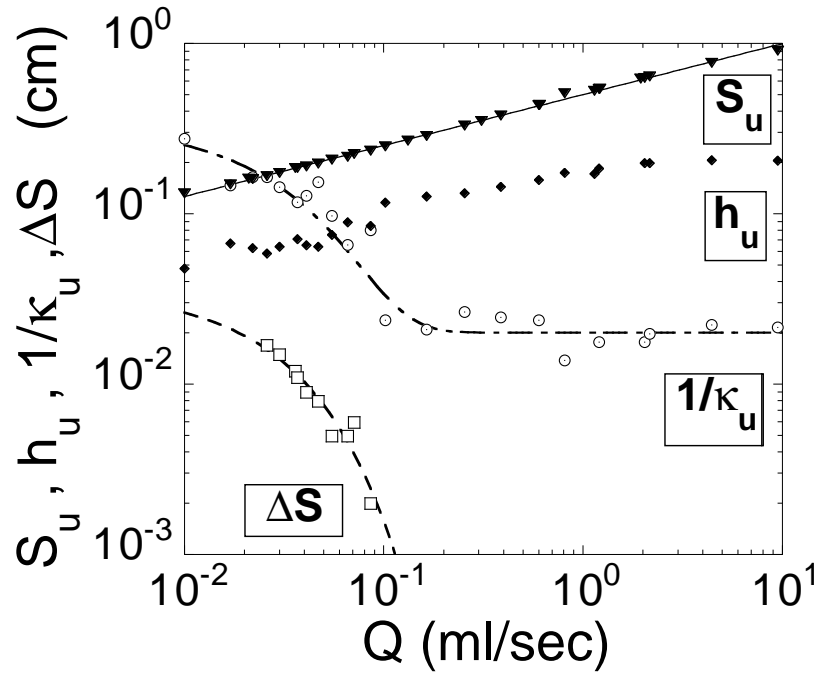


Figure 4: Plots of the transition tube height,  $S_u$ , hysteresis,  $\Delta S$ , transition hump height,  $h_u$ , and transition radius of curvature  $1/\kappa_u$ , as a function of the flow rate  $Q$ .  $S_u \propto Q^{0.3 \pm 0.05}$  (solid line). The  $\Delta S$  data is fit with an exponential decay (dashed) of the form:  $\Delta S = 0.04 \exp^{-Q/0.032}$  although the range is not sufficient to exclude a power-law decay. The mean radius of curvature,  $1/\kappa_u$  is fit (dash dot) with the form:  $1/\kappa_u = 0.02 + 0.32 \exp^{-Q/0.032}$ . This figure is reproduced from Cohen & Nagel (?).

at which point the system makes another discontinuous jump (depicted by the downward dashed arrow) to a part of the sheet where  $q = 0$ . The separation between the two arrows along the  $S$  axis corresponds to  $\Delta S$ . As the diagram indicates, at large values of  $Q$  and  $S$ , the amplitude of the fold or equivalently  $\Delta S$  decreases dramatically.

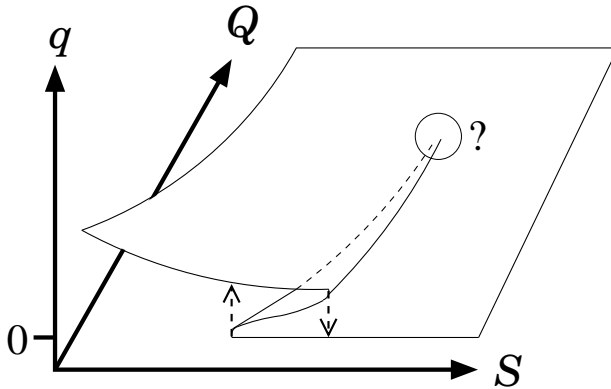


Figure 5: Bifurcation diagram summarizing the features of the selective withdrawal transition. The vertical axis labeled  $q$  depicts the amount of the lower fluid withdrawn as a function of the withdrawal rate  $Q$  and straw height  $S$ . The folded two dimensional sheet represents the states which are accessible to the system. The fold represents the amount of hysteresis in the transition which becomes too small to measure at large enough  $Q$  and  $S$ .

It is unclear whether at high enough  $Q$  or  $S$  the system undergoes a bifurcation where the hysteresis vanishes, or if there always remains some small fold in the sheet which is too small to be detected by the experiments. It seems unlikely that the transition could have a cut-off (and remain discontinuous) and yet have no hysteresis. Such a situation would entail the disappearance of the hump solutions at the exact location in the parameter space where the spout solutions emerge. It is likely that numerical investigations which are able to detect both stable and unstable solutions will be needed in order to answer this question definitively. The exponential decay in both the  $\Delta S$  and  $1/\kappa_u$  curves suggests that even if there does exist a small amount of hysteresis at large  $S$  or  $Q$ , there is a separate and localized mechanism that generates the transition hysteresis at low values of  $S$  or  $Q$ .

When transitions occur at low  $S$  or  $Q$ , the ratio of the withdrawal tube diameter,  $D$ , over the straw height,  $S$ , is of order one. As a result, the circulation rolls set up by withdrawal press against the two-fluid interface and the streamlines near the hump tip become distorted. By changing the flow geometry, the straw diameter sets a length scale for the hump mean radius of curvature at the transition,  $1/\kappa_u$ . Figure 6 shows the effect of a factor of five increase in  $D$  on the  $S_u$  and  $1/\kappa_u$  curves. For the range of flow rates explored,  $\Delta S$  is always about

an order of magnitude smaller than  $S_u$ . Therefore, it is not surprising that the two  $S_u$  curves in figure 6 show no significant dependence on  $D$ . On the other hand, the  $1/\kappa_u$  data show that the onset of the flat asymptotic dependence for  $1/\kappa_u$  occurs at higher  $Q$  for larger straw diameters. This evidence indicates that the hysteresis observed in the experiments results from the finite width of the withdrawal tube. At large values of  $S_u$  these finite size effects vanish. We therefore restrict our scaling analysis to this regime.

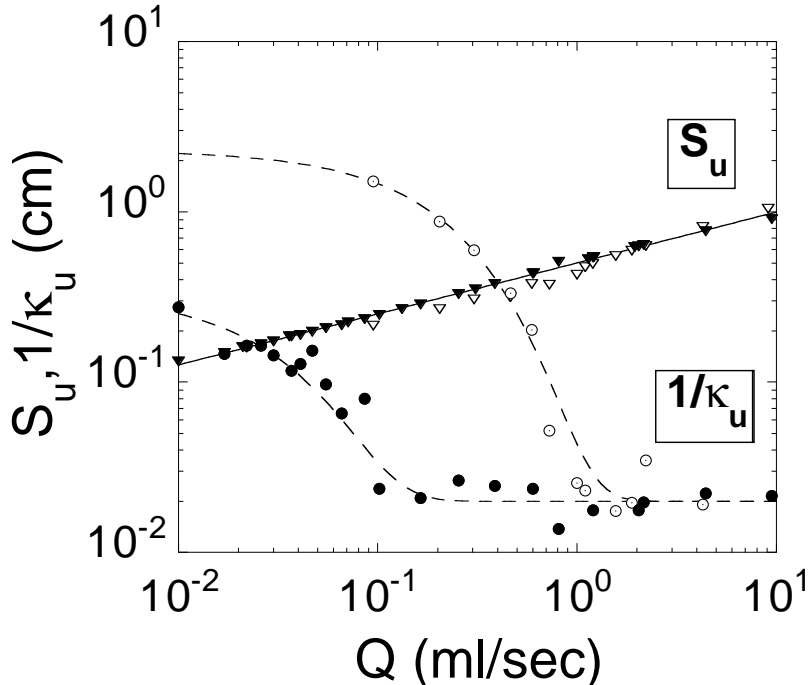


Figure 6: Dependence of the  $S_u$  and  $1/\kappa_u$  vs.  $Q$  curves on the withdrawal tube diameter,  $D$ . The closed symbols reproduce the  $S_u$  and  $\kappa_u$  curves in figure 4 where  $D = 0.16$  cm. The open symbols depict the values of  $S_u$  and  $\kappa_u$  as a function of  $Q$  when  $D = 0.79$  cm. The solid line is a fit to the  $D = 0.16$  data which shows that  $S_u \propto Q^{0.3 \pm 0.05}$ . The mean radius of curvatures,  $1/\kappa_u$  are fit (dash) with the forms:  $1/\kappa_u = 0.02 + 0.32 \exp^{-Q/0.032}$  and  $1/\kappa_u = 0.02 + 2.3 \exp^{-Q/0.22}$  for the  $D = 0.16$  and  $D = 0.79$  cm data sets respectively.

## 4 Scaling Analysis And Similarity Solutions

Although the cut-off in the transition exists even for high values of  $Q$ , Cohen & Nagel (?) showed that the separation in length scales between the hump radius of curvature and the boundary conditions is sufficient for the system to

display scaling and a similarity solution near the transition. As mentioned in the introduction, in the 2-D analogue to the selective withdrawal problem the viscosity of the lower fluid,  $\nu_l$ , greatly affected the observed scaling dependencies. In order to determine the effects of  $\nu_l$  on the transition structure in the present 3-D problem, a comparison of the scaling behavior for two systems with different values of  $\nu_l$  is presented below.

Figure 7 reproduces the Cohen and Nagel scaling curves for the hump curvature and height for system 6 while figure 8 shows the results of an identical treatment performed on data taken for system 5 (where  $\nu_l$  is two hundred times smaller). Figures 7a and 8a, show a plot of the mean curvature at the hump tip,  $\kappa$  (where  $0 \leq \kappa \leq \kappa_u$ ), as a function of  $Q$  for six representative data sets each of which corresponds to measurements taken at a different fixed straw height  $S$ . All of the curves display a steep rise in the curvature with increasing  $Q$ . The insets to figures 7a and 8a show that, as the flow rate approaches  $Q_c$  (used as a fitting parameter), the steep rise in the curvatures takes the form of power-law divergences with exponents of about -0.84 and -0.80 respectively. For each fluid system, all of the data sets (15 sets for large  $\nu_l$  system and 20 for low  $\nu_l$  system) have the same power-law exponent for the divergence. However, the power-law prefactors,  $c_\kappa(S)$ , change with  $S$ . These prefactors are scaled out in the insets for clarity.

Figures 7b and 8b, show a plot of the hump height,  $h_{max}$  (where  $0 \leq h_{max} \leq h_u$ ), as a function of  $Q$  for six data sets each of which corresponds to measurements taken at a different fixed straw height  $S$ . The insets to figures 7b and 8b show that as the flow rate approaches  $Q_c$  (obtained from insets to figures 7a and 8a), the hump heights approach the height  $h_c$  (used as a fitting parameter) as power-laws with exponents of about 0.73 and 0.70 respectively. While the curves for each fluid system show that  $h_{max}$  approaches  $h_c$  with the same power-law exponent, the power-law prefactors  $c_h(S)$  change with  $S$ . These prefactors are scaled out in the insets for clarity.

We combine the two scaling dependencies in figures 7c and 8c and plot  $\frac{h_c - h_{max}}{h_{max}}$  as a function of the normalized curvature  $\frac{\kappa}{n}$ . The normalization constant,  $n$ , scales out the power-law prefactors for curves corresponding to different straw heights. The two figures show that  $\frac{h_c - h_{max}}{h_{max}}$  scales as  $(\frac{\kappa}{n})^\beta$  where  $\beta = -0.85 \pm 0.09$  for the high  $\nu_l$  system and  $\beta = -0.86 \pm 0.10$  for the low  $\nu_l$  system. These results indicate that for this range of straw heights, both fluid systems show no change in the power-law exponent  $-\beta$  even though the height  $h_c$  and the power-law prefactor  $n$  change with  $S$ .

Note that  $n(S) = c_h(S)[c_\kappa(S)^\beta]$ . The constants  $n(S)$  decreases roughly as  $\exp^{-2.5S}$  for both systems. While both systems have the same form for the decay of the constants  $n(S)$ , in the lower  $\nu_l$  system, the values of  $n(S)$  are larger by about ten percent. Also, as indicated by table 1, the asymptotic value of  $k_u$  at the high  $Q$  regime is different by about a factor of 1.5. A detailed analysis of table 1 described in Section 6 suggests that these very slight differences are attributable the different values  $\Delta\rho$  in the two systems. This comparison demonstrates that the lower fluid viscosity  $\nu_l$  does not affect the scaling relations near the selective withdrawal transition.

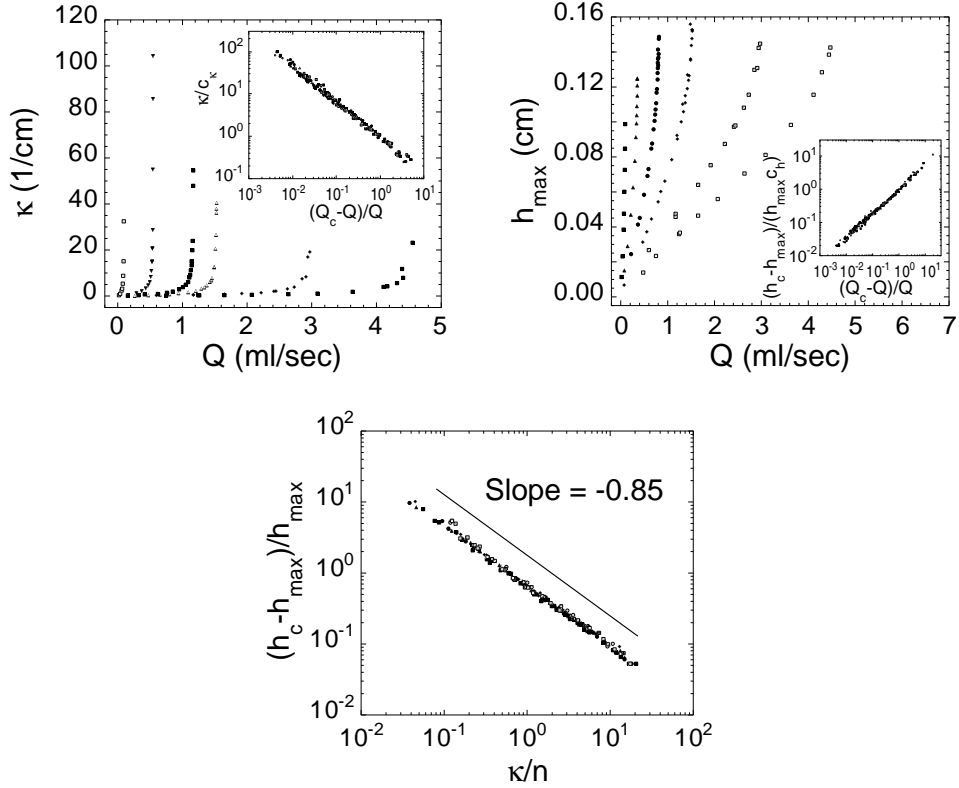


Figure 7: Scaling for the hump mean curvature,  $\kappa$ , and height  $h_{max}$ . Figure 7a plots  $\kappa$  vs.  $Q$  for six tube heights. Each curve displays diverging behavior with increasing  $Q$ . For each tube height, a critical flow rate,  $Q_c$ , is chosen as a fitting parameter so that as  $Q$  approaches  $Q_c$ , the curvatures increase as power laws with an exponent of about -0.84 (7a inset). The prefactors to the curvature power laws,  $c_\kappa(S)$ , are scaled out in the inset. Figure 7b plots  $h_{max}$  vs.  $Q$ . For each  $S$ , a critical hump height,  $h_c$ , is chosen as a fitting parameter. As the flow rate approaches  $Q_c$  (obtained from 7a inset), the hump heights approach the critical heights as power-laws with an exponent about 0.73. The prefactors,  $c_h(S)$ , to the power laws in the inset are scaled out. Figure 7c plots  $(h_c - h_{max})/h_{max}$  vs.  $\kappa/n$  for the entire data set corresponding to fifteen different straw heights. The prefactor  $n$  roughly decreases as  $\exp^{-2.5S}$ . The line corresponds to a power-law with an exponent of -0.85. This figure is reproduced from Cohen & Nagel (?).

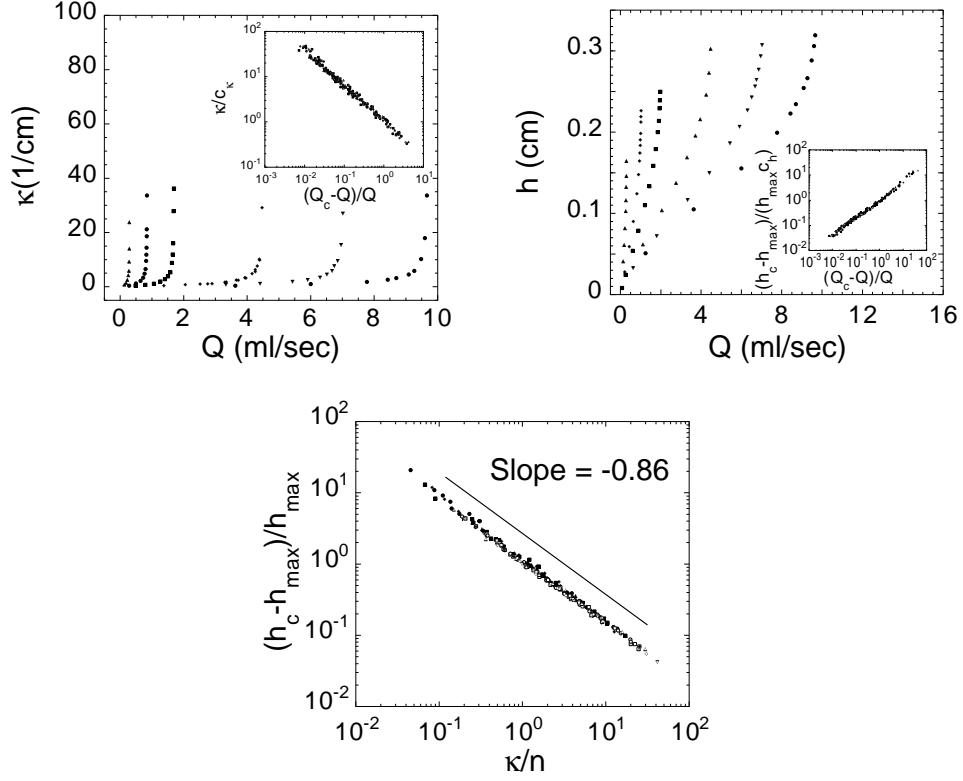


Figure 8: Scaling for the hump mean curvature,  $\kappa$ , and height  $h_{max}$ . Figure 8a plots the  $\kappa$  vs.  $Q$  for six tube heights. Each curve displays diverging behavior with increasing  $Q$ . For each tube height, a critical flow rate,  $Q_c$ , is chosen as a fitting parameter so that as  $Q$  approaches  $Q_c$ , the curvatures increase as power laws with an exponent of about -0.80 (8a inset). The prefactors to the curvature power laws,  $c_\kappa(S)$ , are scaled out in the inset. Figure 8b plots  $h_{max}$  vs.  $Q$  for six tube heights. For each  $S$ , a critical hump height,  $h_c$ , is chosen as a fitting parameter. As the flow rate approaches  $Q_c$  (obtained from 8a inset), the hump heights approach the critical heights as power-laws with an exponent of about 0.70. The prefactors,  $c_h(S)$ , to the power laws in the inset are scaled out. Figure 8c plots  $(h_c - h_{max})/h_{max}$  vs.  $\kappa/n$  for the entire data set corresponding to twenty different straw heights. The prefactor  $n$  roughly decreases as  $\exp^{-2.5S}$ . The line corresponds to a power-law with an exponent of -0.86.

The scaling analysis shows that the hump profiles behave as though they are approaching a singular solution where, at the flow rate  $Q_c$  the hump height would be equal to  $h_c$  and the mean curvature,  $\kappa$ , would diverge. The transition cuts off the evolution of the hump states preventing the system from getting arbitrarily close to the singularity and limiting the precision with which the power-law exponents can be determined.  $Q_c$  changes with  $S$  indicating that the system can approach a continuous line of singularities which closely tracks the hump to spout transition curve in the  $S$  vs.  $Q$  parameter space.

Cohen & Nagel (?) showed that the scaling relations for the hump height and curvature can be used to collapse the hump profiles near the transition onto a universal curve. The quantities  $\frac{n}{\kappa}$  and  $\frac{h_c - h_{max}}{h_{max}}$  track how quickly the radial and axial length scales decrease as the system approaches the singularity. In accordance with the definitions of Cohen and Nagel, the scaled variables are defined as:

$$H(R) = \frac{h_c - h(r)}{h_c - h_{max}} \quad \text{and} \quad R = \frac{r\kappa}{n}, \quad (1)$$

Here  $h(r)$  is the hump profile and the value of  $h_c$  is taken from the scaling relations. This transformation shifts and scales the profiles so that the singularity is located at the origin and the maximum hump heights are located at  $H = 1$  and  $R = 0$ . Figure 9 reproduces the similarity analysis of Cohen and Nagel (system 6) for the hump profiles near the transition while figure 10 shows the results of an identical treatment performed on data taken for the small  $\nu_l$  system (system 5).

Figures 9 and 10 show a series of eight scaled profiles for the  $S = 0.830$  cm data set in the large  $\nu_l$  system and the  $S = 0.667$  cm data set in the small  $\nu_l$  system. The bottom insets in the figures show an overlay of the different hump profiles which are scaled in the main figures. Both figures display excellent collapse for the hump profiles. The solid lines are power-laws which fit the scaled profiles in the region beyond the parabolic hump tips. The scaling relation in figures 7 and 8 can be used to predict the exponent,  $x$ , in the power-law fits. Inserting the observed scaling dependence  $\frac{h_c - h_{max}}{h_{max}} = \left(\frac{\kappa}{n}\right)^\beta$  into the observed form  $H(R) = R^x$  which fits the profile, the following relation is obtained:

$$\frac{h_c - h(r)}{h_{max}} \left(\frac{\kappa}{n}\right)^{-\beta} = r^x \left(\frac{\kappa}{n}\right)^x. \quad (2)$$

Since, for a given  $r$ , the functions  $\frac{h_c - h(r)}{h_{max}}$  and  $r^x$  have constant values,  $x$  must equal  $-\beta$ . More intuitively, as  $Q$  is increased, the parabolic tip regions decrease their radial length scale and are simultaneously pulled towards the singularity in the axial direction leaving behind power-law profiles with exponents that reflect the rate at which these length scales are decreasing. The fits to the profiles indicate that  $x = 0.72 \pm 0.08$  and  $x = 0.72 \pm 0.10$  for the high and low  $\nu_l$  systems respectively. Both of these exponents are within error (although slightly smaller) of the exponent observed in the scaling relation of figures 7 and 8 which, respectively, predict values of  $0.85 \pm 0.09$  and  $0.86 \pm 0.10$  for  $x$ .



Typically, the observed scaling dependencies in these types of problems result from the local stress balance. A scaling analysis where the viscous stresses of the upper and lower fluids balance the stress arising from the interfacial curvature predicts linear scaling dependencies and conical profile shapes. The non-linearity of the observed dependencies and the lack of dependence of the similarity solution on  $\nu_l$  indicate that a different stress balance may govern the flows (e.g. only viscous stress due to upper fluid balances stress due to the interface curvature). Furthermore, non-local effects coupling themselves into the solution could account for the slight differences between the values of the exponents  $\beta$  and  $x$ . Further evidence for the existence of these coupling effects is presented in section 6.

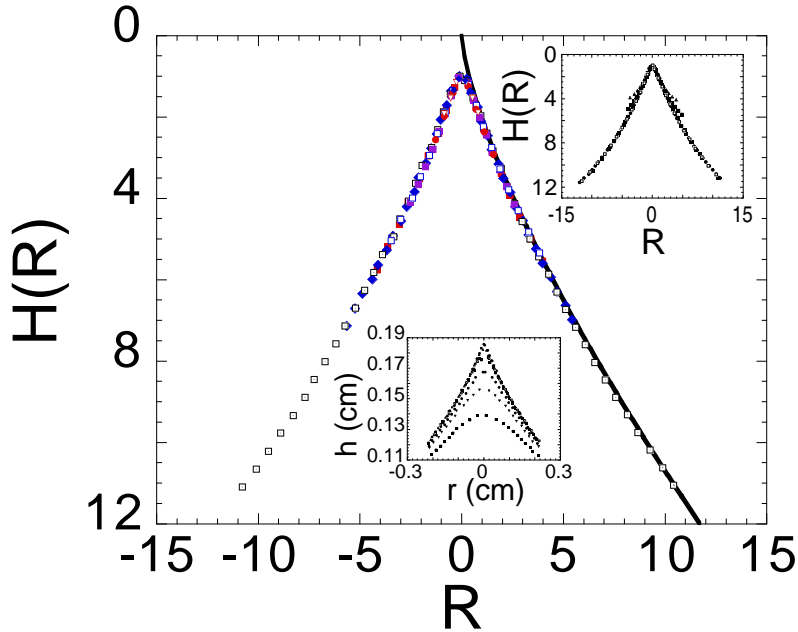


Figure 9: The scaled hump profiles for system 6. The lower inset shows eight profiles taken from the  $S = 0.830$  data set. The main figure shows the same profiles after scaling. The solid line corresponds to a power law of the form  $R^{0.72}$ . In the upper inset we compare the universal curves for the  $S = 0.830$  cm, 0.613 cm, 0.508 cm, 0.381 cm, 0.255 cm data sets. This figure is reproduced from Cohen & Nagel (?).

In both figures, the upper right inset shows a comparison of the similarity solutions for five different tube heights. The profiles corresponding to the different tube heights all display the same power-law dependence. Within error,  $\frac{k}{n}$  (taken from figures 7 and 8) can be used to scale the radial components of these profiles and obtain good collapse. Recall that the normalization prefac-

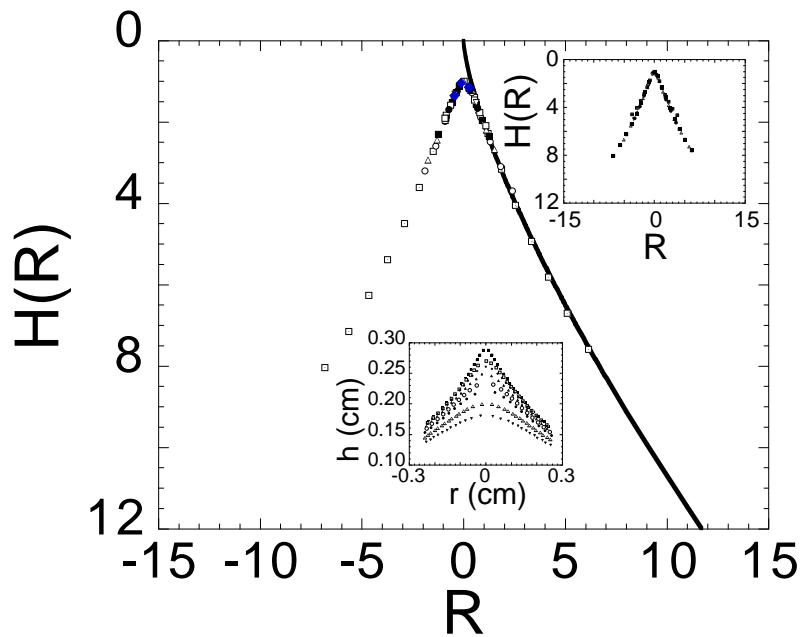


Figure 10: The scaled hump profiles for system 5. The lower inset shows eight profiles taken from the  $S = 0.667$  data set. The main figure shows the same profiles after scaling. The solid line corresponds to a power law of the form  $R^{0.72}$ . In the upper inset we compare the universal curves for the  $S = 0.984$  cm, 0.921 cm, 0.889 cm, 0.667 cm, 0.445 cm data sets.

tors  $n(S)$  decrease roughly as  $\exp^{-2.5S}$ . Here, this decrease is correlated with the observation that the profiles become shallower at larger  $S$ . The points of deviations for the  $S = 0.255$  cm and 0.381 cm profiles in the large  $\nu_l$  system, and the  $S = 0.445$  cm profile in the small  $\nu_l$  system, mark the transition from the similarity regime to the matching regime beyond which the profiles become asymptotically flat. At large enough radii all of the scaled profiles display these deviations.

As a final check, figure 11 shows a comparison of the similarity profile for  $S = 0.831$  cm in the large  $\nu_l$  system and the similarity profile for  $S = 0.667$  cm in the small  $\nu_l$  system. An error analysis calculation<sup>3</sup> for the data points located between  $-5 < R < 5$  (where the residuals are centered around zero - see figure 11) shows that  $\chi^2 \approx 1.6$ . This  $\chi^2$  value indicates that the differences between the two similarity curves are on the same order as the experimental uncertainty which is taken to be a quarter of a scaled pixel. The excellent collapse verifies that  $\nu_l$  and the viscosity ratio do not affect the similarity solution and emphasizes that the scaling behavior observed in these systems is robust.

## 5 Mapping Out The Transition Location

Having shown that the viscosity ratio does not affect the scaling relations and self-similarity characterizing the detailed structure of the transition, I return to the question of whether  $S_u$  is affected by such a change in parameters. There is a large body of work dating back to the late 1940's (see, for example, Rouse (1956); Gariel (1949); Craya (1949); Muskat (1972)) which addresses the mapping out of the selective withdrawal transition location. A large portion of this work focuses on the problem of extracting crude oil deposits without withdrawing any of the water which is often trapped beneath the oil. Nearly all of the experimental studies found in the literature which address these large scale extraction problems assume that the flows have a high Reynolds number or, equivalently, that the viscous stresses are negligible. Therefore, low viscosity fluids were used to model the flows. One exception arises in the modeling by Blake & Ivey (1986) of magma layer mixing during volcanic eruptions. However, as described earlier, miscible fluids were used in those investigations. Since, as Lister (1989) showed, the absence of surface tension allows for the withdrawal of both fluids at any withdrawal rate, these particular studies never addressed the actual selective withdrawal transition. With the advent of new technologies

<sup>3</sup>Since the data points for both curves were not aligned,  $\chi^2$  was calculated in the following way: First a local linear fit was used to interpolate the value of curve<sub>1</sub> between the data points. Second, the minimum distance between the interpolated curve and the value of the points in curve<sub>2</sub>,  $\delta_{i,2}$  was calculated. The  $\chi^2$  value for the entire curve is defined as:  $\chi^2 = \frac{1}{N} \sum \frac{\delta_{i,2}^2}{\sigma_{1x}^2 + \sigma_{1y}^2 + (\sigma_{2x}^2 + \sigma_{2y}^2)/n}$  where  $N$  is the number of points compared,  $\sigma_{1x}$  and  $\sigma_{1y}$  are the experimental errors associated with the  $x$  and  $y$  points in curve<sub>1</sub>,  $\sigma_{2x}$  and  $\sigma_{2y}$  are the experimental errors associated with the  $x$  and  $y$  points in curve<sub>2</sub>,  $n$  is equal to the number of points used in making the linear fit to curve<sub>1</sub>, and the sum is taken over the index  $i$  which labels the points in curve<sub>2</sub>.

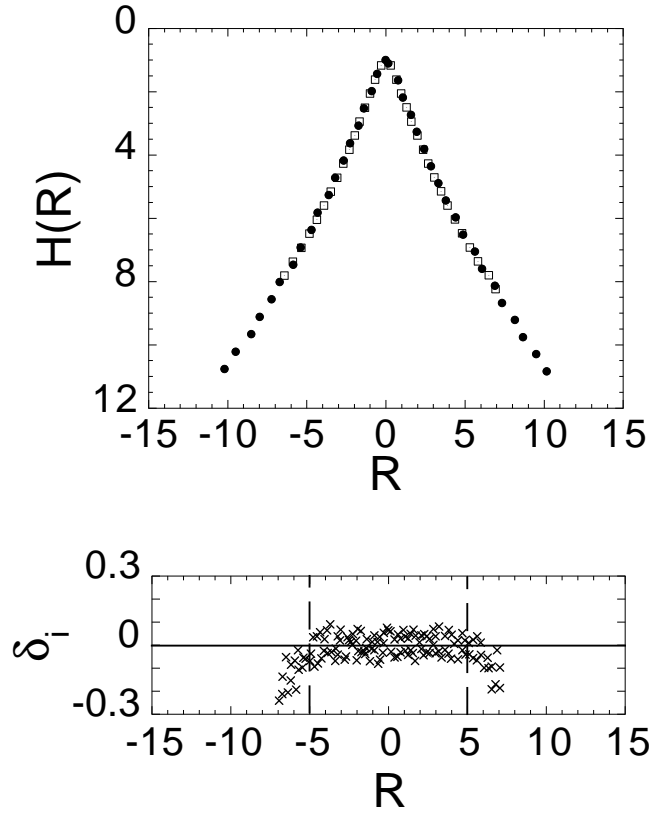


Figure 11: Comparison of the similarity profiles for systems 5 and 6. The closed symbols correspond to the  $S = 0.830$  cm data for system 6 while the open symbols correspond to the  $S = 0.667$  cm data for system 5. Figure 11b shows a plot of residual quantity,  $\delta_i$  for all of the data points. Here,  $\delta_i$  is the minimum distance between each point on the system 6 curve and the value of a local linear fit to the system 5 curve at the same  $R$  value. The region between the vertical dotted lines corresponds to the similarity regime where the residuals become centered around zero. The  $\chi^2$  calculation was performed within this similarity regime.

which use the selective withdrawal geometry in conjunction with low Reynolds number flows (see, for example, Cohen *et al.* (2001); Ganan-Calvo (1998)), it has become increasingly important to determine the effect of the viscous stresses on the transition.

Figure 12 shows a plot of  $S_u$  versus  $Q$  for seven pairs of fluids. Table 1 lists the fluids used in making these measurements along with the measured values of the interfacial tension,  $\gamma$ , the fluid densities,  $\rho_u$  and  $\rho_l$ , the density mismatch,  $\Delta\rho$ , the fluid viscosities,  $\nu_u$  and  $\nu_l$ , and the viscosity ratio  $\nu_l/\nu_u$ .

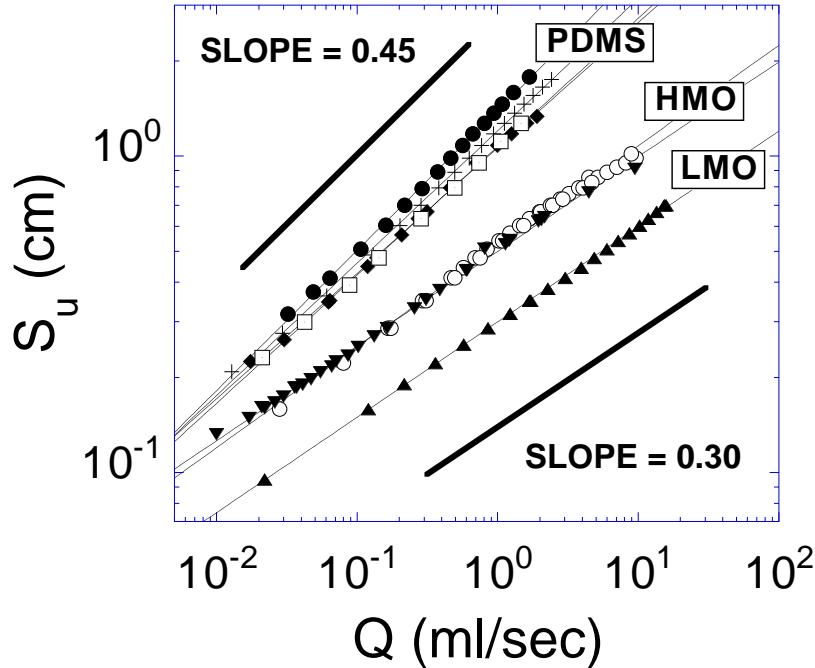


Figure 12: Plots of the transition tube height  $S_u$  as a function of  $Q$  for the seven systems listed in table 1. Table 1 lists the symbol used in plotting the  $S_u$  curve for each system. For each system, it is observed that  $S_u \propto Q^\alpha$  where the power  $\alpha$  (listed in table 1) ranges between 0.30 and 0.45. The  $S_u$  curves cluster into three groups which correspond to the three different upper fluids used in the experiments. Each cluster is labeled with the corresponding upper fluid.

There are a few obvious trends. First, all of the data sets show that  $S_u \propto Q^\alpha$  where the power  $\alpha$  ranges between 0.30 and 0.45. The last row in Table 1 shows the value of the exponent for the power-law used to fit the  $S_u$  curves for each system. Second, for a given value of  $Q$ , an increase in  $\nu_u$ , the upper fluid viscosity, increases  $S_u$ . The three distinct clusters of curves in figure 12 correspond to three distinct upper fluid viscosities. As figure 12 shows, a five fold increase in  $\nu_u$  can increase  $S_u$  by a factor of two. Third, for a given value of  $Q$ , even a thousand fold increase in the lower fluid viscosity does not significantly

affect  $S_u$ . These last two observations indicate that it is the upper fluid viscosity rather than the viscosity ratio which affects the transition location within the  $S$  vs.  $Q$  parameter space.

The remaining trends in the data are weak. In order to ascertain the effects of the surface tension,  $\gamma$ , and density mismatch,  $\Delta\rho$  on the transition straw height, these parameters must be varied by large amounts. Unfortunately, reducing  $\gamma$  below about 20 dynes/cm causes mixing of the fluid layers and results in a diffuse interface under high shear rates. Therefore it is very difficult to vary  $\gamma$  in the experiments by more than a factor of two. Another difficulty arises from an inability to decouple the changes in these parameters for different systems. For example, when comparing systems 1 and 4, an order of magnitude increase in  $\Delta\rho$  is coupled with a factor of two decrease in  $\gamma$ . Since both  $\Delta\rho$  and  $\gamma$  act to stabilize the interface, the effects due to these variations may cancel. A further complication arises due to the effect of surfactant concentration on the interface. As will be discussed in Appendix A, the accumulation of surfactants on the interface tend to shift  $S_u$  by an amount which is comparable to the slight shifts seen in top four curves (which form the uppermost cluster) in figure 12. More careful measurements of  $S_u$  are necessary in order to resolve these weaker trends.

It is instructive to compare these results with currently available theoretical predictions for the transition which take into account both the viscous stresses and the surface tension. While there are no current numerical studies which have been tailored to address this exact problem, the closest approximation to such a treatment can be found in the Lister (1989) paper on selective withdrawal for zero Reynolds number flow. While his simulations were performed for equal viscosity fluids, the fact that the lower fluid viscosity is irrelevant to the transition location can be used to compare the simulations with the experiments for which the fluid viscosities are unequal. Since those simulations were designed to address large scale magma flows rather than the small scale fluid flows found in the experiments, care must be taken in making a comparison of the results. For example, the simulations were designed to model a system with a point sink which is located many capillary lengths (defined as  $\sqrt{\frac{\gamma}{\Delta\rho g}}$ ) away from the interface. However in the experiments,  $S$  is comparable to the capillary length. Thus, the experiments are performed at much smaller values of  $Q$  and  $S_u$  than the simulations making it impossible to quantitatively compare the results. Nevertheless, since it is expected that  $S_u$  is a smooth function of  $Q$ , one can check that the two data sets are consistent with this expectation.

Another issue which needs to be addressed is the determination of the Reynolds number for the experimental flows. There are a variety of ways in which the Reynolds number can be defined. The greatest change in the velocity of the upper fluid occurs along the line connecting the tip of the hump and the withdrawal tube. Since the fluid at the tip of the hump is stationary the magnitude of this change in velocity is  $\frac{Q}{\pi(D/2)^2}$ . The distance of the tube orifice to the interface is the largest length scale affecting the flows<sup>4</sup>. Therefore, the quantity

<sup>4</sup>For this range of flow rates and density mismatch values, the capillary length scale is a

$Re_{max} = \frac{QS}{\pi(D/2)^2\nu}$  can be used as an upper bound for the Reynolds number. In figure 12, the upper most cluster of  $S_u$  curves has  $0.005 < Re_{max} < 6$ , the middle cluster of curves has  $0.03 < Re_{max} < 50$ , and the lowest curve has  $0.05 < Re_{max} < 350$ . These estimates imply that a comparison with results from a zero Reynolds number simulation must be treated with caution. For example, the effects of the fluid's inertia could manifest themselves as a change in  $\alpha$ , the value of the exponent for the power-law fits in figure 12<sup>5</sup>. Such an explanation could account for the decrease in  $\alpha$  which occurs when  $\nu_u$  is decreased from 10 St to 1.9 St. However, since an equally large change in Reynolds number can occur along the  $S_u$  versus  $Q$  curves it is curious that kinks which may be indicative of such a change are not observed.

In figure 13 the  $S_u$  vs.  $Q$  curves are compared with the predictions of Lister for systems with  $\nu_u = 10$  St,  $\nu_u = 1.9$  St, and  $\nu_u = 0.57$  St corresponding to systems 4, 6 and 7 in table 1. The solid and open symbols denote data from the experiments and simulations respectively. The dashed lines represent power-law fits to the experimental results. These fits are projected into the regime for which the simulations have a prediction for the value of  $S_u$ . Since Lister's simulations were performed using dimensionless variables, the proper values for the fluid parameters were used to determine the values of  $S$  and  $Q$ . Furthermore, the simulation flow rate is reduced by a factor of two in order to make a first order correction for the fact that the simulations use a point sink rather than a tube to withdraw the fluids.

There are two features of the comparison which need be addressed. First, the simulations curves for the  $\nu_u = 10$  St system fall below the projected power-laws. In Section 3 evidence was provided for the lack of dependence of  $S_u$  on the straw diameter  $D$  for the range of flow rates used in the experiments. Therefore it is unclear whether geometric factors alone could account for the large shift which is necessary for the collapse of the numerical results onto the projected experimental power-laws. Second, it is disturbing that the power-law exponents for the systems which use less viscous (rather than more viscous) upper fluids agree more favorably with the zero Reynolds number simulation results. As stated above, the shift in the power-law exponent for the experimental results indicates that there may be more than one way to balance the stresses acting on the interface. The simulation results only address the regime where surface tension and buoyancy effects play an equal role in stabilizing the interface and therefore do not observe the change in the  $S$  vs.  $Q$  power-law exponents<sup>6</sup>. Nevertheless, the fact that the simulations predict a power law exponent of one third and the fact that the experimentally measured exponents are centered around this value deserves notice.

Finally, it is often possible to use the scaling relations observed in systems approaching a singularity to help identify which stresses are balancing each other. Such an identification for the different fluid systems could in turn help

---

little smaller than  $S$ . However, it is conceivable that for a set of density matched fluids or for measurements at very small  $S$  the capillary length could become larger than  $S$ .

<sup>5</sup>W. W. Zhang private communication.

<sup>6</sup>W. W. Zhang private communication.

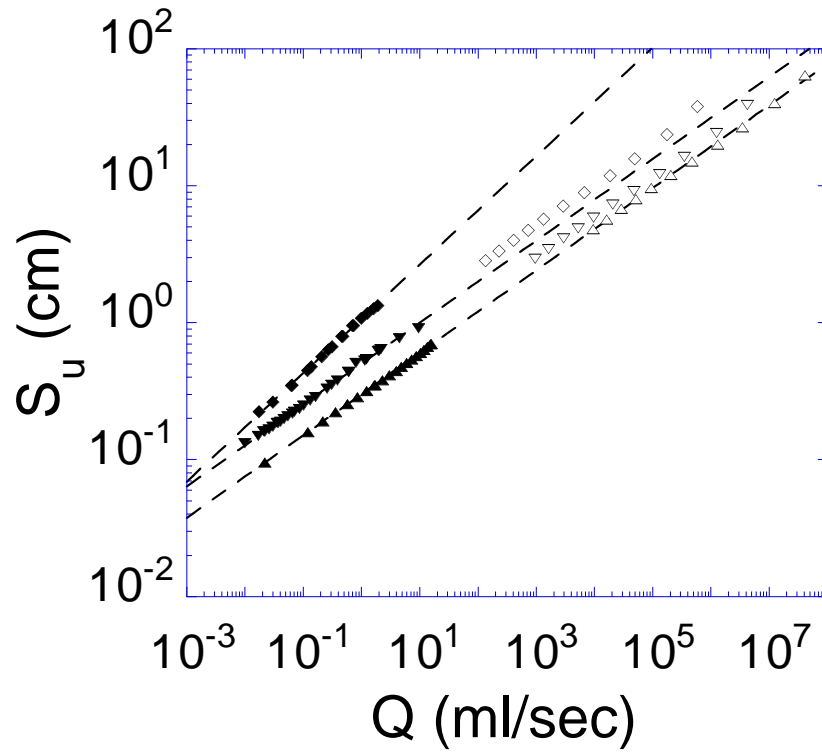


Figure 13: Comparison of the experimentally measured  $S_u$  curves for systems 4, 6, and 7 in Table 1 with those predicted by the simulations of Lister (1989). The closed symbols depict the experimental measurements while the corresponding open symbols depict the simulation predictions for a system with the same fluid parameters. The dashed lines are power-law fits to the experimental data.



explain the observed changes in the exponent  $\alpha$ .

## 6 Conclusions

In this paper, it has been shown that the transition straw height for a given flow rate,  $S_u$ , changes as:  $S_u \propto Q^\alpha$ , where  $\alpha$  ranges between about 0.45 and 0.30. This is the first instance in which experiments comparing  $S_u$  for different systems of immiscible fluids with flows in the low Reynolds number regime have been performed. The data indicates that for the selective withdrawal system, the upper fluid viscosity rather than the viscosity ratio determines the value of  $S_u$ . It has been shown, that when the withdrawal tube is sufficiently close to the interface, the transition is hysteretic: the straw height at which the spout collapses back into a hump is different from  $S_u$ . At larger straw heights, the difference between  $S_u$  and the spout to hump transition straw height,  $\Delta S$ , decays exponentially. This effect has been linked to the tube diameter which at low  $S$ , sets a length scale for the final mean radius of curvature  $1/\kappa_u$ . However, the transition remains discontinuous and  $\kappa_u$  remains finite even at large  $S$ .

I have performed a detailed comparison of the scaling relations for two systems which have the same upper fluid viscosity but have a lower fluid viscosity which is different by a factor of two hundred. The surface tension for the two systems was different by about 13% while the density mismatch was different by a factor of three (See systems 5 and 6 in table 1). It is observed that up until the cutoff, the hump profiles behave as though they are approaching a singular solution where, at the flow rate  $Q_c$  the hump height would be equal to  $h_c$  and the mean curvature,  $\kappa$ , would diverge. The quantity  $\frac{h_c - h_{max}}{h_{max}}$  has been shown to scale as  $(\frac{k}{n})^\beta$  where  $\beta = -0.85 \pm 0.09$  for the high  $\nu_l$  system and  $\beta = -0.86 \pm 0.10$  for the low  $\nu_l$  system. These scaling relation were used to collapse the hump profiles for different flow rates and straw heights near the transition onto a single universal curve. The region of the similarity profiles located beyond the parabolic tip can be fit with a power law which has an exponent  $x = 0.72$  for both systems. The results show that both the scaling exponents and the shape of the similarity solution are independent of  $\nu_l$  and the viscosity ratio. In fact, a direct comparison of the similarity solution for both fluid systems indicates that, within error, the curves are identical.

As described in the introduction, in the 2-D analogue to the selective withdrawal problem the lower fluid viscosity plays a fundamental role in determining how close the system can approach the cusp singularity. In the 3-D selective withdrawal system, the asymptotic value of  $\kappa_u$  shows little or no dependence on  $\nu_l$ . Therefore, the effects of the lower fluid viscosity must enter as higher order terms which are undetected by the experiments. Since  $\kappa_u$  is independent of the flow rate at large  $S$ , an increase in the Capillary number,  $\nu_u \frac{Q}{r^2} / \gamma$  can also be ruled out as a method of getting the system closer to the singularity.

The saturation value of the mean curvature,  $\kappa_{usat}$  does show some dependence on the upper fluid viscosity  $\nu_u$ . For example, systems 5 and 7 in table 1 show that when  $\gamma$  and  $\Delta\rho$  are kept constant, decreasing  $\nu_u$  from 2.0 St to 0.57

St, decreases  $\kappa_{usat}$  by a factor of six. However, as systems 2 and 5 in the table indicate, this trend is not uniform. Shallow hump profiles are also observed for nearly inviscid systems which use air as the upper fluid and water as the lower fluid. Therefore, it is likely that one of the ways in which  $nu_u$  can affect  $\kappa_{usat}$  is by shifting the balance between the viscous and inertial terms in the governing Navier-Stokes equations. For the remaining systems which have a lower Reynolds number characterizing the flows, even a factor of five increase in  $nu_u$  does not significantly affect  $\kappa_{usat}$ .

Since at low enough Reynolds numbers the fluid viscosities do not affect  $\kappa_{usat}$ , the only remaining parameters which may act to set the length scale for the cutoff are the density mismatch  $\Delta\rho$  and surface tension  $\gamma$ . With the exception of systems 1 and 6, the large error in the data makes it difficult to distinguish between the  $\kappa_{usat}$  values for the different systems. Also, the trends in the data are too weak to allow for a determination of the effects of  $\gamma$  on  $\kappa_{usat}$ . However, a comparison of system 1 with systems 2, 3, and 4 and a comparison of system 6 with system 5 indicates that an increase in  $\Delta\rho$  results in a higher value for  $\kappa_{usat}$ . Note that for both comparisons  $\nu_u$  is kept constant. This result is intriguing since the similarity treatment for the profiles is localized to the hump tip whereas the effects of the density mismatch should only affect the system on a length scale comparable to the capillary length  $\sqrt{\frac{\gamma}{\Delta\rho g}}$ . These observations suggest that the matching region which connects the profile near the tip of the hump to the flat interface at large radii is responsible for setting the length scale for the cutoff<sup>7</sup>. Such an effect could also explain the slight difference between the observed value of the power-law exponent describing the similarity solution( $x$ ) and the value predicted by the scaling relations( $\beta$ ). The importance of identifying which parameters determine the length scale for the cutoff warrants a more careful investigation of the  $\kappa_{usat}$  dependence on  $\Delta\rho$ ,  $\gamma$  and the local interfacial boundary conditions.

The robustness of the similarity analysis shows that singularities can be used to organize the study and classification of the steady state hump profiles near the selective withdrawal transition. In particular, the discontinuous nature of the transition, marked by the cut-off curvature  $\kappa_u$ , coupled with the display of scaling behavior suggests a transition structure which is remarkably similar to that of weakly-first-order thermodynamic transitions. Whether this analogy hints at some deeper relationship between the classification schemes for weakly first order thermodynamic transitions and those for these types of topological transitions remains to be shown.

I am grateful to S. R. Nagel, W. W. Zhang, S. Venkataramani, J. Eggers, H. A. Stone, D. Mueth, J. Wyman, T. J. Singler, H. A. Lyden, J. N. Israelachvili, C. C. Park, S. Chaieb, V. Putkaradze, R. Parthasarathy, S. N. Coppersmith, T. A. Witten, L. P. Kadanoff, P. Constantin, R. Scott, E. Blucher, T. Dupont, H. Diamant, and V. C. Prabhakar for sharing their insights and their help with editing this manuscript. This research is supported by the University of Chicago

<sup>7</sup>J. Eggers, W. W. Zhang, S. R. Nagel, J. Wyman, and H. A. Stone (private communication).

(MRSEC) NSF DMR-9808595 and NSF DMR-0089081 grants.

## A Surfactant effects

Surfactants are chimeric molecules consisting of hydrophobic and hydrophilic sections which tend to aggregate at fluid interfaces<sup>8</sup>. Even under very controlled conditions, it is difficult to keep fluid systems free of surfactants for long periods of time. Since, surfactants can significantly affect the interfacial tension and surface flows, part of understanding the details of any fluid interface problem entails isolating and accounting for the effects of surfactants.

In the present studies there are two types of effects which are thought to result from the presence of surfactants. First, for a given flow rate, it is observed that over a period of several days,  $S_u$  increases by a small amount indicating that the surface tension in the system may have been uniformly reduced. Second, at the transition, the system oscillates between the hump state and the spout state over a period of about minute<sup>9</sup> in a manner similar to that observed by de Bruijn (1993) in tip streaming of drops under shear flow. In the tip streaming experiments, a straining flow stretches a drop of fluid so that the two tips of the drop (each of which is analogous to the hump tip) have a high curvature. At sufficiently high shear rates the drop can enter the streaming state (analogous to the spout state) where a small jet of fluid emanates from each of the drop tips. It is observed that near the transition the drops oscillate between the stretched drop state and the streaming state. This oscillatory behavior has been linked to the accumulation of surfactants near the stagnation point located at the drop tip. This accumulation lowers the local surface tension and causes a transition to the streaming state. The jet “sweeps” the interface, reduces the local concentration of surfactants, and subsequently collapses back into the drop state at which point the cycle begins again. While the local boundary conditions for this problem are different from those of the selective withdrawal problem, the flow patterns are remarkably similar indicating that the oscillatory behavior observed in both systems may be correlated. Below, I explain how both of these effects influence the results presented in the main body of this paper.

Figure 14 shows plots of  $S_u$  vs.  $Q$  for three data sets corresponding to measurements performed on system 6. The filled down-triangles correspond to measurements taken just after the fluid interface was cleaned<sup>10</sup>. The open down-triangles, correspond to measurements of  $S_u$  taken after the surfactant

---

<sup>8</sup>For some oil-oil (for example Polybutadiene and PDMS) interfaces the random thermal energy is able to keep the surfactants off the interface. However these systems usually have a very low surface tension and therefore develop diffuse interfaces under high shear rates.

<sup>9</sup>Note that the time scale for this effect is much larger than the time scale for the pump induced noise in the withdrawal rate which can produce a similar effect when the system is very close to the transition.

<sup>10</sup>When the system is in the spout state, surfactants, which have accumulated on the interface are “swept” into the straw and deposited in the waste container. By leaving the system in the spout state for long periods of time, the surfactant concentration over the entire interface can be significantly reduced.

concentration at the interface was allowed to equilibrate for a period of a week. A uniform 20% increase in  $S_u$ , or, equivalently, a 50% decrease in the transition flow rate is observed. Upon cleaning the interface once again, the  $S_u$  data points return to their original value (open diamonds). Note that the observed shift in  $S_u$  resulting from the differing surfactant concentration is quite small compared with the shift observed when  $\nu_u$  is increased by a factor of five. Nevertheless, the fact that the transition flow rate can change by nearly 50% depending on the surfactant concentration is noteworthy. Finally, in figure 15, a comparison between the  $\frac{h_c - h_{max}}{h_{max}}$  vs.  $\frac{\kappa}{n}$  curves for the equilibrated system (squares) and the clean system (open circles) indicates that the shift in  $S_u$  does not affect the scaling relations.

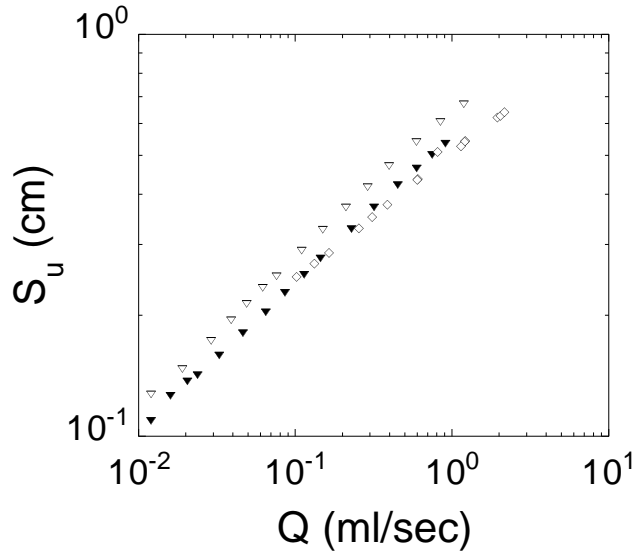


Figure 14: Plots of the transition tube height  $S_u$  as a function of  $Q$  for system 6 in Table 1. The filled down-triangles correspond to measurements taken just after the interface was cleaned. The open down-triangles correspond to measurements taken after the surfactant concentration at the interface was allowed to equilibrate over a period of a week. The open diamonds correspond to measurements taken after the system was cleaned once again.

While the increase in the  $S_u$  values is most likely due to a uniform reduction in  $\gamma$  over the entire interface, the dynamic nature of the observed hump to spout oscillations implies that (as with tip streaming) the flows may cause local variations in the surfactant concentration. In this picture, when the system is in the hump state, surfactants are dragged towards the hump tip by the surface flows. If the system is sufficiently close to the transition, this accumulation, which lowers the surface tension locally, causes the hump to increase its height and curvature and ultimately drives the system into the spout state. Once in the spout state, the local surfactant concentration reduces over time and the

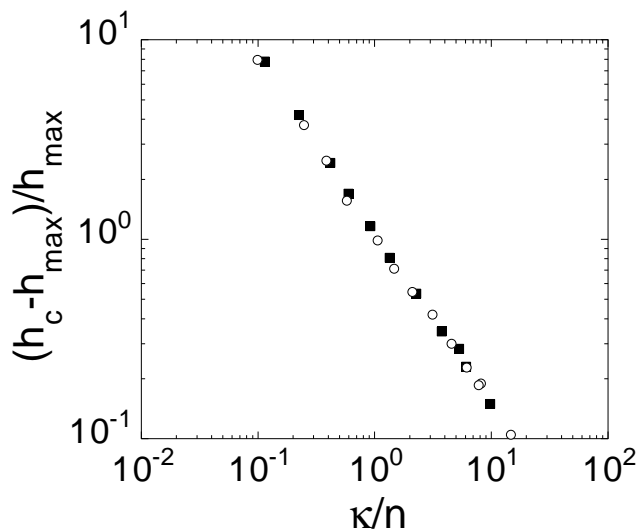


Figure 15: Plots of  $\frac{h_c - h_{max}}{h_{max}}$  vs.  $\frac{\kappa}{n}$  for system 6 in Table 1. The squares correspond to measurements taken after the surfactant concentration at the interface was allowed to equilibrate over a period of a week. The open circles correspond to measurements taken after the system had been cleaned.

system eventually decays back into the hump state. The detailed characteristics of this cyclical behavior depend on the surfactant concentration over the entire interface.

When the entire interface has been cleaned, it takes a long time for the surfactants to accumulate in concentrations large enough to affect the steady state. Therefore, the increase in the hump curvature and height is slow. Furthermore, once the interface forms a spout, it takes a very short amount of time for the local concentration of surfactants to be reduced. Consequently, systems that have been cleaned spend a very small fraction of the hump to spout oscillation cycle in the spout state. Since many of the measurements discussed in the paper were performed in the vicinity of the transition, care needed to be taken when measuring the hump height and curvature. In order to understand how  $h_{max}$  and  $\kappa$  change with time, the following experiment was performed. First, the system was placed in the hump state. Then, the flow rate was increased momentarily so that the interface formed a spout for a short period of time. Just after spout collapse, the time dependence of the hump curvature and height was measured. Figures 16a and 16b show the results of measurements performed for the same system, with the same value of  $S$ , but at different values of  $Q$ . The initial decay, which occurs over a time scale of about five seconds, gives some measure of the relaxation time for the flows in these systems. Following this initial decay, the height and curvature values plateau. These plateaus are associated with a regime where the local surfactant concentration is too low to

affect the shape of the interface. When the system is near the transition so that  $\frac{Q_c - Q}{Q} \approx 0.004$ , the plateau regime is short lived (about fifteen seconds) and is followed by a regime in which both the height and curvature increase their values (figure 16a). However, when the experiments are performed at larger values of  $\frac{Q_c - Q}{Q}$  the plateau regime is longer. Figure 16b shows that when  $\frac{Q_c - Q}{Q} \approx 0.01$  the plateau regime lasts for over twenty minutes.

When collecting data for the scaling relations, it is important to determine the value of the hump height and mean curvature in the plateau regime. Also, a larger amount of error must be assigned to data points taken from plateau regimes that are short lived. Note however that since the plateau regime lengthens quite rapidly as  $\frac{Q_c - Q}{Q}$  is increased, for the cleaned interface, these precautions only apply to the one or two data points in the scaling relations, which are closest to the transition.

While all of the scaling data presented in the main body of this paper was taken for clean interfaces, it is useful to understand the changes in the transition structure which occur when the surfactant concentration has been allowed to equilibrate over a period of days. For equilibrated interfaces the increase in the hump height and curvature occurs over a shorter amount of time so that the plateau regimes shorten. Therefore, greater caution needs to be taken in the measurements of the scaling relations. However as figure 15 shows, when such precautions are taken no noticeable changes in the scaling relations are observed.

Another characteristic of the equilibrated systems, is that (unlike the cleaned systems) they can spend a large fraction of the hump to spout oscillation cycle in the spout state. During the time which the system spends in the spout state, it is possible (even at high  $Q$  or  $S$ ) to quickly raise the straw and cause the spout to collapse back into the hump state<sup>11</sup>. The amount  $\Delta S$  necessary to cause the collapse can be measured. I find that the value of  $\Delta S$  varies depending on conditions. For example, if the  $\Delta S$  measurement is performed just after the local concentration of surfactants has been reduced, only a small amount of hysteresis is observed. On the other hand if the experiment is performed after the concentration of surfactants has been allowed to build up,  $\Delta S$  can become as large as  $80 \mu\text{m}$ . Note that even this large amount of hysteresis is orders of magnitude smaller than the typical value of the straw height and therefore does not significantly affect the  $S_u$  vs.  $Q$  curves for the equilibrated system.

In conclusion, it is observed that allowing the surfactant concentration to equilibrate over a period of days has a relatively small effect (20% increase) on the  $S_u$  measurements (figure 14) and, when the proper precautions are taken, no effect on the scaling relations (figure 15).

<sup>11</sup>Since the spout drains the lower fluid, the straw height  $S$  increases with time. Therefore, it is necessary to check that the amount of hysteresis is actually larger than the increase in  $S$  which occurs during the time it takes to perform the measurement.

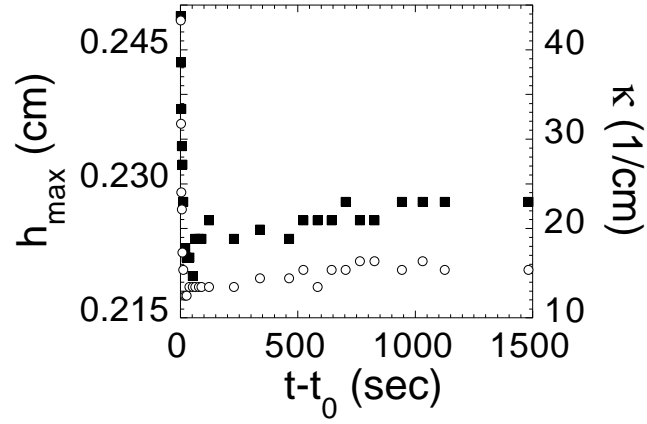
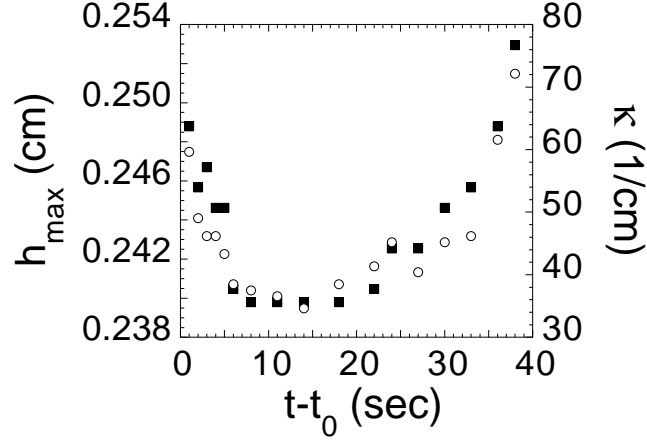


Figure 16: Plots of the time dependence for  $h_{max}$  (squares) and  $\kappa$  (open circles) just after spout collapse for system 3 in Table 1. The figures correspond to measurements taken at constant  $S$  but at different  $Q$ s. In both figures,  $t_0$  corresponds to the time at which the spout collapses into a hump. Figure 16a shows measurements for a system which is very close to the transition with  $\frac{Q_c-Q}{Q} \approx 0.004$ . Figure 16b shows measurements for a system which is slightly farther away from the transition with  $\frac{Q_c-Q}{Q} \approx 0.01$ .

## References

- ACRIVOS, A. & LO, T. S. 1978 Deformation and breakup of a single slender drop in an extensional flow. *J. Fluid Mech.* **86**, 641–672.
- BARENBLATT, G. I. 1996 *Scaling, self-similarity and intermediate asymptotics*. Cambridge, UK: Cambridge University Press.
- BEAR, J. 1972 *Dynamics of Fluids in Porous Media*. New York: McGraw-Hill.
- BENSIMON, D., KADANOFF, L. P., LIANG, S., SHRAIMAN, B. & TANG, C. 1986 Viscous flows in 2 dimensions. *Rev. Mod. Phys.* **58**, 1986.
- BERTOZZI, A. L., BRENNER, M. P., DUPONT, T. F. & KADANOFF, L. P. 1994 *Trends and Perspectives in Applied Mathematics*. New York: Springer.
- BLAKE, S. & IVEY, G. N. 1986 Magma-mixing and the dynamics of withdrawal from stratified reservoirs. *J. Volcanol. & Geotherm. Res.* **27**, 153–178.
- DE BRUIJN, R. A. 1993 Tipstreaming of drops in simple shear flows. *Chem. Eng. Sci.* **48**, 277–284.
- C AFLISCH, R. E. & PAPANICOLAOU, G. C. 1993 In *Singularities in Fluids, Plasmas, and Optics*. Norwell, MA: Kluwer.
- COHEN, I., LI, H., HOUGLAND, J. L., MRKSICH, M. & NAGEL, S. R. 2001 Using selective withdrawal to coat microparticles. *Science* **292**.
- COHEN, I. & NAGEL, S. R. ? Scaling at the selective withdrawal transition. ?  
?, ?
- COHEN, I. & NAGEL, S. R. 2001 Testing for scaling behavior dependence on geometrical and fluid parameters in the two fluid drop snap-off problem. *Phys. of Fluids* **13**, 3533–3541.
- CRAYA, A. 1949 Recherches theoretiques sur l'ecoulement de couches superposees de fluides de densites differentes. *La Houille Blanche* **4**, 44–55.
- EDGERTON, H. E., HAUSER, E. A. & TUCKER, W. B. 1937 *J. Phys. Chem.* **41**, 1209.
- EGGERS, J. 1997 Nonlinear dynamics and breakup of free-surface flows. *Rev. Mod. Phys.* **69**, 865.
- EGGERS, J. 2001 Air entrainment through free-surface cusps. *Phys. Rev. Lett.* **86**, 4290.
- GANAN-CALVO, A. M. 1998 Generation of steady liquid microthreads and micron-sized monodisperse sprays in gas streams. *Phys. Rev. Lett.* **80**, 285–288.



- GARIEL, P. 1949 Recherches experimentales sur l'écoulement de couches superposees de fluides de densites differentes. *La Houille Blanche* **4**, 56–64.
- GOLDSTEIN, R. E., PESCI, A. I. & SHELLEY, M. J. 1993 Topology transitions and singularities in viscous flows. *Phys. Rev. Lett.* **70**, 3043.
- HALE, J. K. & COCAK, H. 1991 *Dynamics and Bifurcations*. New York: Springer-Verlag.
- HANSEN, F. K. & RODSRUD, G. 1991 Surface-tension by pendant drop .1. a fast standard instrument using computer image-analysis. *J. Colloid Interface Sci.* **141**, 1.
- HARELMAN, D. F., MORGAN, R. L. & PURPLE, R. A. 1959 In *Selective withdrawal from a vertically stratified fluid. Proc. 8th Congress Int. Assoc. Hydraulic Res.*, pp. 10-C-1-10-c-16.
- JEONG, J. T. & MOFFATT, H. K. 1992 Free-surface cusps associated with flow at low reynolds number. *J. Fluid Mech.* **241**, 1–22.
- JIRKA, G. H. & S., K. D. 1979 Supercritical withdrawal from two layered fluid systems. part 2: Three-dimensional flow into a round intake. *J. Hydraul. Res.* **17**, 53–62.
- LISTER, J. R. 1989 Selective withdrawal from a viscous two-layer system. *J. Fluid Mech.* **198**, 231–254.
- LISTER, J. R. & STONE, H. A. 1998 Capillary breakup of a viscous thread surrounded by another viscous fluid. *Phys. Fluids* **10**, 2758–2764.
- MUSKAT, M. 1972 *Physical Principles of Oil Production*. New York: McGraw-Hill.
- NAGEL, S. R. & ODDERSHEDE, L. 2000 Singularity during the onset of an electrohydrodynamic spout. *Phys. Rev. Lett.* **85**, 1234.
- NEUMANN, A. W. & SPELT, J. K. 1995 *Applied Surface Thermodynamics*. New York: Marcel Dekker.
- PUGH, M. & SHELLEY, M. J. 1998 *Comm. Pure App. Math.* **51**, 733.
- ROUSE, H. 1956 Development of the non-circulatory waterspout. *J. Hydraul. Div. Proc. Am. Soc. Civil. Eng.* **82**, 1038.3–1038.7.
- SEGUR, J. B. & OBERSTAR, H. E. 1951 viscosity of glycerol and its aqueous solutions. *Ind. Eng. Chem.* **43**, 2117.
- SHERWOOD, J. D. 1984 Tip streaming from slender drops in a nonlinear extensional flow. *J. Fluid Mech.* **144**, 281–295.
- ZEFF, B. W., KLEBER, B., FINEBERG, J. & LATHROP, D. P. 2000 Singularity dynamics in curvature collapse and jet eruption on a fluid surface. *Nature* **403**, 401.